Mon. Not. R. Astron. Soc. **000**, 000–000 (0000) Printed 22 July 2011 (MN LATEX style file v2.2)

Gamma Ray Bursts in the comoving frame

G. Ghirlanda [1⋆], L. Nava[2], G. Ghisellini[1], A. Celotti[2], D. Burlon[3], S. Covino[1], A. Melandri[1]
[1]*INAF – Osservatorio Astronomico di Brera, Via E. Bianchi 46, I-23807 Merate, Italy*
[2]*SISSA – via Bonomea, 265, I-34136 Trieste, Italy*
[3]*Max-Planck-Institut für Extraterrestrische Physik, Giessenbachstraße 1, D-85478 Garching, Germany*

ABSTRACT
We estimate the bulk Lorentz factor Γ_0 of 32 GRBs using the measured peak time of their afterglow light curves. We consider two possible scenarios for the estimate of Γ_0: the case of a homogeneous circumburst medium or a wind density profile. The values of Γ_0 are broadly distributed between few tens and several hundreds with average values $\sim$125 and $\sim$63 for the homogeneous and wind density profile, respectively. We find that the isotropic energy and luminosity correlate in a similar way with Γ_0, i.e. $E_{\rm iso}\propto{\Gamma_0}^2$ and $L_{\rm iso}\propto{\Gamma_0}^2$, while the peak energy $E_{\rm peak}\propto\Gamma_0$. These correlations are less scattered in the wind density profile than in the homogeneous case. We then study the energetics, luminosities and spectral properties of our bursts in their comoving frame. The distribution of $L'_{\rm iso}$ is very narrow with a dispersion of only one decade in the wind case, clustering around $L'_{\rm iso}\sim 5\times10^{48}$ erg s^{-1}. Peak photon energies cluster around $E'_{\rm peak}\sim$ 5 keV. The newly found correlations involving Γ_0 offer a general interpretation scheme for the spectral–energy correlation of GRBs. The $E_{\rm peak}-E_{\rm iso}$ and $E_{\rm peak}-L_{\rm iso}$ correlations are due to the different Γ_0 factors and the collimation–corrected correlation, $E_{\rm peak}-E_\gamma$ (obtained by correcting the isotropic quantities for the jet opening angle $\theta_{\rm j}$), can be explained if $\theta_{\rm j}^2\Gamma_0=$ constant. Assuming the $E_{\rm peak}-E_\gamma$ correlation as valid, we find a typical value of $\theta_{\rm j}\Gamma_0\sim$ 5–12, in agreement with the predictions of magnetically accelerated jet models.

Key words: Gamma-ray: bursts — Radiation mechanisms: non thermal

1 INTRODUCTION

The discovery of the afterglows of Gamma Ray Bursts (GRBs - Costa et al. 1997) allowed to pinpoint their position in the X–ray and Optical bands. This opened a new era focused at measuring the spectroscopic redshifts of these sources. The present[1] collection of GRBs with measured z consists of 232 events. In 132 bursts of this sample (updated in this paper) the peak energy $E^{\rm obs}_{\rm peak}$ of their νF_ν prompt emission γ–ray spectrum could be constrained. In turn, for these bursts it was possible to calculate the isotropic equivalent energy $E_{\rm iso}$ and luminosity $L_{\rm iso}$. The knowledge of the redshifts showed that two strong correlations exist between the *rest frame* peak energy $E_{\rm peak}$ and $E_{\rm iso}$ or $L_{\rm iso}$ (also known as the "Amati" and "Yonetoku" correlations – Amati et al. 2002, Yonetoku et al. 2004, respectively).

The reality of these correlations has been widely discussed in the literature. Some authors pointed out that they can be the result of observational selection effects (Nakar & Piran 2005; Band & Preece 2005; Butler et al. 2007, Butler, Kocevski & Bloom 2009; Shahmoradi & Nemiroff 2011) but counter–arguments have been put forward arguing that selection effects, even if surely present, play a marginal role (Ghirlanda et al. 2005, Bosnjak et al. 2008, Ghirlanda et al. 2008; Nava et al., 2008; Krimm et al. 2009; Amati et al. 2009). The finding that the a correlation $E_{\rm p}(t)$–$L_{\rm iso}(t)$ exists when studying time–resolved spectra of individual bursts is a strong argument in favor of the reality of the spectral energy correlations, (Ghirlanda, Nava& Ghisellini 2010; Ghirlanda et al. 2011) and motivates the search for the underlying process generating them. Even if several ideas have been already discussed in the literature, there is no general consensus yet, and a step forward towards a better understanding both of the spectral energy correlations and the underlying radiation process of the prompt emission of GRBs is to discover what are the typical energetics, peak frequencies and peak luminosities in the *comoving frame*.

The physical model of GRBs requires that the plasma emitting γ–rays should be moving relativistically with a bulk Lorentz factor Γ_0 much larger than unity. The high photon densities and the short timescale variability of the prompt emission imply that GRBs are optically thick to pair production which, in turn, would lead to a strong suppression of the emitted flux, contrary to what observed. The solution of this compactness problem requires that GRBs are relativistic sources. From this argument lower limits $\Gamma_0\geqslant100$ are usually derived (Lithwick & Sari, 2001). The first observational evidences supporting this scenario were found in the radio band where the ceasing of the radio flux scintillation (few weeks after

⋆ E-mail:giancarlo.ghirlanda@brera.inaf.it
[1] http://www.mpe.mpg.de/∼jcg/grbgen.html

the explosion as in GRB 970508; Frail et al. 1997), allowed to estimate Γ of a few. This value corresponds to the late afterglow phase, when the fireball is decelerated almost completely by the interstellar medium and is characterized by a much smaller bulk Lorentz factor than the typical Γ_0 of the prompt phase.

Large Lorentz factors imply strong beaming of the radiation we see. We are used to consider GRB intrinsic properties ($E_{\rm peak}$, $E_{\rm iso}$, $L_{\rm iso}$) for the bursts with measured redshifts, but still an important correction should be applied. Our aim is to study the distributions of $E_{\rm peak}$, $E_{\rm iso}$, $L_{\rm iso}$ and the spectral–energy correlations ($E_{\rm peak}-E_{\rm iso}$ and $E_{\rm peak}-L_{\rm iso}$) in the *comoving frame*, accounting for the Γ_0 factor. The estimate of Γ_0 is possible by measuring the peak of the afterglow (Sari & Piran 1999) and has been successfully applied in some cases (e.g. Molinari et al. 2007, Gruber et al., 2011) and more extensively recently by Liang et al. (2010) in the optical and X–ray band. Other methods allow to set lower limits (Abdo et al. 2009; Ackerman et al. 2010; Abdo et al. 2009a) mainly by applying the compactness argument to the high energy emission recently detected in few GRBs at GeV energies by the *Fermi* satellite (see Zou, Fan & Piran 2011; Zhao, Li & Bai 2011; Hascoet et al. 2011 for more updated calculation on these lower limits on Γ_0). Conversely, upper limits (Zou & Piran 2010) can be derived by requiring that the forward shock emission of the afterglow does not appear in the MeV energy band.

The paper is organized as follows: in § 2 we discuss the relativistic corrections that allow us to derive the comoving frame $E'_{\rm peak}$, $E'_{\rm iso}$and $L'_{\rm iso}$ from the rest frame $E_{\rm peak}$, $E_{\rm iso}$, $L_{\rm iso}$; in § 3,4 we derive a general formula for the estimate of Γ_0 from the measurement of the time of the peak of the afterglow emission; in § 5 we present our sample of GRBs and in § 6 our results which are finally discussed in § 7. Throughout the paper we assume a standard cosmology with $h=\Omega_\Lambda=0.7$ and $\Omega_m=0.3$.

2 FROM THE REST TO THE COMOVING FRAME

In this section we derive the Lorentz transformations to pass from rest frame quantities to the same quantities in the comoving frame. This is not trivial, since, differently from the analog case of blazars, the emitting region is not a blob with a mono–directional velocity, but a fireball with a radial distribution of velocities. Therefore, an observer located on axis receives photons from a range of viewing angles, complicating the transformations from rest frame to comoving quantities. We are interested to three observables: the peak energy $E_{\rm peak}$, the isotropic equivalent energy $E_{\rm iso}$ and the isotropic equivalent peak luminosity $L_{\rm iso}$. Dealing with isotropic equivalent quantities, we can assume that the emitting region is a spherical shell with velocities directed radially. We also assume that the comoving frame bolometric intensity I' is isotropic. We then adopt the usual relation between observed (I) and comoving (I') bolometric intensity:

$$I = \delta^4 I'; \qquad \delta = \frac{1}{\Gamma(1-\beta\cos\theta)} \tag{1}$$

where δ is the Doppler factor and θ is the angle between the velocity vector and the line of sight. The received flux is

$$F = 2\pi I' \int_0^\pi \delta^4 \sin\theta d\theta \tag{2}$$

Since the fluence $\mathcal{F}$ is a time–integrated quantity we have $\mathcal{F}\propto\int_0^\pi\delta^3\sin\theta d\theta$, i.e. one power of δ less.

$E_{\rm peak}$ — This quantity can be derived from the time–integrated spectrum, or can be the spectral peak energy of a given time interval. In this paper we will use the time–integrated $E_{\rm peak}=E^{\rm obs}_{\rm peak}(1+z)$. The received fluence $d\mathcal{F}/d\theta$ (i.e. the flux integrated in time) from each annulus of same viewing angle θ is $d\mathcal{F}/d\theta\propto\sin\theta\delta^3$. For $\theta\rightarrow 0$ the Doppler factor is maximum, but the solid angle vanishes, while for $\theta>1/\Gamma$ the solid angle is large, but δ is small. Therefore there will be a specific angle θ for which $d\mathcal{F}/d\theta$ is maximum. This is given by

$$\cos\theta=\beta+\frac{2}{5\Gamma^2} \tag{3}$$

At this angle the beaming factor is

$$\delta=\frac{5}{3}\Gamma \tag{4}$$

We then set $E'_{\rm peak}=E_{\rm peak}/(5\Gamma/3)$.

$E_{\rm iso}$ — This is proportional to the fluence $\mathcal{F}$, and the relation between the observed and comoving quantity is

$$\frac{E_{\rm iso}}{E'_{\rm iso}}=\frac{\mathcal{F}}{\mathcal{F}'}=\frac{\int_0^\pi\delta^3\sin\theta d\theta}{\int_0^\pi\sin\theta d\theta}=\Gamma \tag{5}$$

We then set $E'_{\rm iso}=E_{\rm iso}/\Gamma$.

$L_{\rm iso}$ — This is proportional to the flux F, so the ratio $L_{\rm iso}/L'_{\rm iso}$ is

$$\frac{L_{\rm iso}}{L'_{\rm iso}}=\frac{F}{F'}=\frac{\int_0^\pi\delta^4\sin\theta d\theta}{\int_0^\pi\sin\theta d\theta}\sim\frac{4}{3}\Gamma^2 \tag{6}$$

We then set $L'_{\rm iso}=L_{\rm iso}/(4\Gamma^2/3)$ (in agreement with Wijers & Galama 1999).

3 ESTIMATE OF THE BULK LORENTZ FACTOR Γ_0

In the thin–shell regime (i.e. for $T_{90}<t_{\rm peak,obs}$, condition satisfied for almost all bursts in our sample) the standard afterglow theory predicts that the peak of the bolometric afterglow light curve corresponds to the start of the fireball deceleration. The deceleration radius is commonly defined as the radius at which the swept up matter $m(r_{\rm dec})$ is smaller by a factor Γ_0 than the initial shell's rest mass $M_0=E_0/(\Gamma_0 c^2)$. Usually, the deceleration time $t_{\rm dec}$ is estimated as $t_{\rm dec}=r_{\rm dec}/(2c\Gamma_0^2)$ (Sari & Piran 1999). This relation is approximate, since it does not consider that the Lorentz factor is decreasing. Some authors consider this relation to estimate Γ_0 from the peak time of the afterglow light curve (Sari & Piran 1999; Sari 1997), while other authors consider that $t_{\rm dec}=r_{\rm dec}/(2c\Gamma^2_{\rm dec})$, where approximately $\Gamma_0\simeq 2\Gamma(r_{\rm dec})$ (Molinari et al. 2007).

We propose here a detailed and general calculation of Γ_0 which extends the estimate to the generic case of a circumburst density profile described by $n=n_0 r^{-s}$. We use the shape of the light curve in two different power–law regimes: the coasting phase when $r\ll r_{\rm dec}$ and $\Gamma(r)=\Gamma_0$, and the deceleration phase when $r_{\rm dec}\ll r\ll r_{\rm NR}$ (where $r_{\rm NR}$ marks the start of the non–relativistic regime). During the deceleration regime the evolution of the Lorentz factor is described by the self–similar solution found by Blandford & McKee (1976):

$$\Gamma=\sqrt{\frac{(17-4s)E_0}{(12-4s)m(r)c^2}} \tag{7}$$

The relation between the radius and the observed time is obtained by integrating the differential equation $dr=2c\Gamma^2(r)dt$ and by considering the exact evolution of Γ with r. From Eq. 6:

$$L_{\rm iso}=\frac{4}{3}\Gamma^2 L'_{\rm iso}=\varepsilon_e\frac{4}{3}\Gamma^2\frac{dE'_{\rm diss}}{dt'} \tag{8}$$

where the dissipated comoving energy $E'_{\rm diss}$ is given by (Panaitescu & Kumar 2000):

$$E'_{\rm diss} = (\Gamma - 1)m(r)c^2 \quad (9)$$

Only a fraction ε_e of the dissipated energy is radiated. We assume that this quantity is small and does not affect the dynamics of the fireball (adiabatic regime). Eq. 8 holds until the emission process is efficient (fast cooling regime).

During the coasting phase $\Gamma = \Gamma_0 \gg 1$ and the luminosity (denoted by $L_{\rm iso,1}$) is:

$$L_{\rm iso,1} = \varepsilon_e \frac{4}{3}\Gamma_0^3 c^2 \frac{dm(r)}{dt'} = \varepsilon_e \frac{4}{3}\Gamma_0^4 c^3 4\pi r^{(2-s)} n_0 m_{\rm p} \quad (10)$$

Since in this phase the Lorentz factor is constant and equal to Γ_0 the relation between the fireball radius and the observed time is

$$r = 2ct\Gamma_0^2$$

As a function of time, the luminosity is:

$$L_{\rm iso,1} = \varepsilon_e \frac{4}{3} 2^{(4-s)} \pi n_0 m_{\rm p} c^{(5-s)} \Gamma_0^{8-2s} t^{2-s} \quad (11)$$

For a homogeneous density medium ($s = 0$) the light curve rises as t^2. The luminosity is instead constant when $s = 2$, which corresponds to the stellar wind density profile.

To derive the luminosity during the deceleration phase we start again from Eq. 8 and Eq. 9. However, in this case Γ is decreasing accordingly to Eq. 7 (but still $\Gamma \gg 1$). We derive:

$$L_{\rm iso,2} = \varepsilon_e \frac{4}{3}\Gamma^2 c^2 \left[\Gamma \frac{dm(r)}{dt'} + m(r)\frac{d\Gamma}{dt'}\right] \quad (12)$$

The first term of the sum in square brackets can be written as

$$\Gamma \frac{dm(r)}{dr}\frac{dr}{dt'} = (3-s)\frac{m(r)}{r}\Gamma^2 c$$

The second term of the sum becomes

$$m(r)\frac{d\Gamma}{dr}\frac{dr}{dt'} = -\frac{3-s}{2}\frac{m(r)}{r}\Gamma^2 c$$

During the deceleration

$$t = \frac{1}{2c}\int \frac{dr}{\Gamma^2} = \frac{r}{2(4-s)c\Gamma^2}$$

where we have used $\Gamma(r)$ given in Eq. 7.

For $\Gamma_0 \gg 1$ the initial energy content of the fireball $E_0 = E_{\rm k} + M_0 c^2 \simeq E_{\rm k}$, where $E_{\rm k}$ is the kinetic energy powering the expansion of the fireball in the ISM during the afterglow phase. If the radiative efficiency η of the prompt phase is small, $E_{\rm k}$ can be estimated from the energetics of the prompt as $E_{\rm k} = E_{\rm iso}/\eta$. We obtain:

$$\begin{aligned} L_{\rm iso,2} &= \varepsilon_e \frac{4}{3}\Gamma^2 c^2 \frac{(3-s)m(r)}{4(4-s)t} \quad (13)\\ &= \varepsilon_e \frac{4}{3}\frac{(17-4s)(3-s)E_{\rm iso}}{4(12-4s)(4-s)\eta} t^{-1} \end{aligned}$$

The peak time of the light curve is the time when the coasting phase ends and the deceleration phase starts and can be estimated by setting $L_{\rm iso,1}(t_{\rm peak}) = L_{\rm iso,2}(t_{\rm peak})$:

$$t_{\rm peak} = \left[\frac{(17-4s)(3-s)E_{\rm iso}}{2^{6-s}\pi n_0 m_{\rm p} c^{5-s}\eta(12-4s)(4-s)\Gamma_0^{8-2s}}\right]^{\frac{1}{3-s}} \quad (14)$$

and inverting this relation to obtain the initial Lorentz factor as a function of the peak time:

$$\Gamma_0 = \left[\frac{(17-4s)(3-s)E_{\rm iso}}{2^{6-s}\pi n_0 m_{\rm p} c^{5-s}\eta(12-4s)(4-s)t_{\rm peak}^{3-s}}\right]^{\frac{1}{8-2s}} \quad (15)$$

where $t_{\rm peak}$ is the peak of the afterglow light curve in the source rest frame, i.e. $t_{\rm peak} = t_{\rm peak,obs}/(1+z)$, and it will be indicated as $t_{\rm p,z}$ hereafter.

While a wind density profile (hereafter W: wind interstellar medium) is expected from a massive star progenitor that undergoes strong wind mass losses during the final stages of its life (Chevalier & Li 1999), it is not possible at the present stage to prefer the W to the homogeneous interstellar medium case (H, hereafter). We already showed (Nava et al. 2006) that the collimation corrected $E_{\rm peak} - E_\gamma$ correlation (so called "Ghirlanda" correlation; Ghirlanda, Ghisellini & Lazzati 2004) has a smaller scatter and a linear slope when computed under the assumption of the W compared to the H case. It is, therefore, important to compare the estimates of Γ_0 and of the comoving frame energetics in these two possible scenarios. The most extensive study of Liang et al. (2010) estimated Γ_0 mostly from the peak of the afterglow light curve in the optical band and in few cases from a peak in the the X–ray band. They considered only the H case and found a strong correlation between Γ_0 and the GRB isotropic equivalent energy $E_{\rm iso}$.

Eq. 11 predicts that the afterglow light curve is flat in the coasting phase, with no peaks. However, this equation neglects pre–acceleration of the circumburst matter due to the prompt emission itself, that can have important consequences, as we discuss below.

4 HOMOGENEOUS OR WIND DENSITY PROFILE?

In the following we will find the initial bulk Lorentz factor Γ_0 for bursts showing a peak in their early afterglow light curve. In the simple case of an homogeneous circumburst density, we expect that the afterglow luminosity $L_{\rm aft} \propto t^2\Gamma^8$, and therefore $L_{\rm aft} \propto t^2$ when $\Gamma = \Gamma_0 =$ constant (Eq. 11). It can be questioned if, in the case of a wind density profile, such a peak occurs, or if the initial light curve is flat (i.e. $\propto t^0$), as suggested by Eq. 11 when $s = 2$.

The derivation leading to Eq. 11 assumes that the circumburst medium is at rest when the fireball impacts through it (i.e. it is an *external* shock). Instead, since the electrons in the vicinity of the burst scatter part of the prompt emission of the burst itself, some radial momentum has to be transferred to the medium (as suggested by Beloborodov 2002). If the velocity acquired by the circumburst matter becomes relativistic, then the fireball will produce an *internal* shock when passing through the medium, with a reduced efficiency.

To illustrate this point, let consider an electron at some distance r from the burst, scattering photons of the prompt emission of energy $E_{\rm peak} = x m_{\rm e} c^2$. In the Thomson limit of the scattering process, this electron will scatter a number τ of prompt photons given by:

$$\tau = \sigma_{\rm T} n_\gamma \Delta r = \frac{\sigma_{\rm T} L_{\rm iso} c t_{\rm burst}}{4\pi r^2 c\, x m_{\rm e} c^2} = \frac{\sigma_{\rm T} E_{\rm iso}}{4\pi r^2 x m_{\rm e} c^2} \quad (16)$$

To evaluate the distance r up to which this process can be relevant, consider at what distance the electrons make a number $\tau \approx (m_{\rm p}/m_{\rm e})/x$ scatterings, namely the distance at which the electrons and their associated protons are accelerated to $\gamma \sim 2$:

$$r(\gamma = 2) \approx \left[\frac{\sigma_{\rm T} E_{\rm iso}}{4\pi m_{\rm p} c^2}\right]^{1/2} \sim 1.9 \times 10^{15} E_{\rm iso,53}^{1/2} \quad {\rm cm} \quad (17)$$

where $E_{\rm iso,53} = 10^{53} E_{\rm iso}$ erg. This distance must be compared with the deceleration radius $r_{\rm dec}$ in the case of a wind density pro-

GRB	z	$E_{\rm peak}$ keV	$E_{\rm iso}$ erg	$L_{\rm iso}$ erg/s	$t_{\rm p,z}$ s	$\Gamma_{\rm H}$	$\Gamma_{\rm W}$	Ref
990123	1.60	2031±161	(2.39±0.28)E54	(3.53±1.23)E53	18	312	182	2
021211	1.006	94±19	(1.1±0.13)E52	(71.3±9.9)E50	<65	⩾98	⩾34	2
050525A	0.606	127±5.5	(2.89±0.57)E52	(9.53±2.5)E51	<58	⩾116	⩾45	2
050820A	2.612	1325±277	(9.75±0.77)E53	(91±6.8)E51	108.17±4.62	142	93	1
050922C	2.198	417±118	(4.53±0.78)E52	(190±2.3)E51	42	138	55	2
060210	3.91	575±186	(4.15±0.57)E53	(59.5±8.0)E51	97	133	77	2
060418	1.489	572±114	(1.28±0.10)E53	(18.9±1.59)E51	60.73 ±0.82	137	65	1
060605	3.78	490±251	(2.83±0.45)E52	(9.5±1.5)E51	83.14 ±2.7	101	41	1
060607A	3.082	575±200	(10.9±1.55)E52	(20±2.7)E51	42.89 ±0.62	153	68	1
060904B	0.703	135±41	(36.4±7.43)E50	(7.38±1.4)E50	271.91±33.75	50	18	1
060908	2.43	479±110	(7.79±1.35)E52	(26±4.6)E51	<38	⩾154	⩾64	2
061007	1.261	902±43	(8.82±0.98)E53	(17.4±2.45E52	34.62 ±0.18	215	121	1
061121	1.314	1289±153	(2.61±0.3)E53	(141±1.5)E51	250	88	54	4
070110	2.352	370±170	(5.5±1.5)E52	(45.1±7.52)E50	350	64	34	4
071003	1.1	1678±231	(1.8±0.14)E53	(84±1.5)E51	<61	⩾143	⩾70	2
071010B	0.947	101±23	(2.12±0.36)E52	(64±0.53)E50	67	105	40	2
080319B	0.937	1261±25	(1.5±0.17)E54	(9.6±0.23)E52	<76	⩾171	⩾113	2
080319C	1.95	1752±505	(15±0.79)E52	(9.5±0.12)E52	117.38±3.22	109	57	1
080810	3.35	1488±348	(3.91±0.37)E53	(9.27±0.87)E52	27.02 ±0.26	214	105	1
080916C	4.35	2759±120	(5.6±0.5)E54	(10.4±0.88)E53	1.5	880	419	3
081203A	2.1	1541±757	(3.5±0.3)E53	(28.1±1.94)E51	118.09±0.46	121	70	1
090510	0.903	4400±400	(5.0±0.5)E52	(1.78±0.12)E53	0.44	773	175	3
090812	2.452	2023±663	(4.03±0.4)E53	(95.6±9.66)E51	17.38	253	118	5
090902B	1.822	2020±17	(44±0.3)E53	(58.9±0.97)E52	3.2	643	327	3
090926A	2.106	907±7	(20±0.52)E53	(74±1.45)E52	2.9	605	275	3
091024	1.092	946±118	(7.2±0.7)E52	(52.4±7.24)E50	1912	35	24	5
091029	2.752	230±66	(7.4±0.74)E52	(13.2±0.73)E51	88	111	51	5
100621A	0.542	146±23.1	(4.37±0.5)E52	(3.16±0.24)E51	3443	26	18	5
100728B	2.106	404±29	(3.0±0.3)E52	(18.6±1.20)E51	16	188	63	5
100906A	1.727	158±16	(3.34±0.3)E53	(24.5±0.86)E51	37	186	93	5
110205A	2.22	715±239	(5.6±0.6)E53	(2.50±0.34)E52	311	89	62	5
110213A	1.46	241±13	(6.4±0.6)E52	(20.9±0.58)E51	81	113	51	5

Table 1. The sample of GRBs with redshifts z, rest frame peak energy $E_{\rm peak}$, isotropic equivalent energy $E_{\rm iso}$ and luminosity $L_{\rm iso}$ (integrated in the 1 keV–10 MeV energy range) and peak time of the afterglow light curve (given in the source rest frame $t_{\rm p,z}$. The Γ_0 factors computed in the H and W case are reported. The last column gives the references for the peak time of the afterglow: (1) Liang et al. 2010, peak of the optical light curve; (2) Liang et al. 2010, references in their Tab. 6; (3) Ghisellini et al. 2010; (4) Ghisellini et al., 2009; (5) GRBs added in this work (Melandri et al. 2011)

file corresponding to a mass loss $\dot{M}$ and a velocity $v_{\rm w}$ of the wind:

$$n(r) = \frac{\dot{M}}{4\pi r^2 m_{\rm p} v_{\rm w}} = 3.16\times10^{35}\frac{\dot{M}_{-5}}{v_{\rm w,8} r^2} \qquad (18)$$

where $\dot{M} = 10^{-5}\dot{M}_{-5} M_\odot\ {\rm yr}^{-1}$ and $v_{\rm w} = 10^8$ cm s^{-1} (i.e. 10^3 km s^{-1}) (see e.g. Chevalier & Li 1999). The deceleration radius is

$$r_{\rm dec} = \frac{E_{\rm iso}}{4\pi m_{\rm p} c^2 \eta \Gamma_0^2} \sim 1.7\times10^{16}\frac{E_{\rm iso,53} v_{\rm w,8}}{\eta_{-1}\dot{M}_{-5}\Gamma^2_{0,2}}\ {\rm cm} \qquad (19)$$

where η is the efficiency of conversion of the kinetic energy to radiation ($L_{\rm iso} = \eta L_{\rm k,iso}$). Therefore it is possible to have a pre–acceleration of the circumburst matter up to a distance comparable to (but less than) the deceleration radius. In this case we expect to have a very early *rising* afterglow light curve (corresponding to relatively inefficient internal shocks between the fireball and the pre–accelerated circumburst medium), followed by a flat light curve and then a decay.

We conclude that the absence of a flat early light curve does not exclude (a priori) a wind density profile. This gives us a motivation to explore both cases (i.e. homogeneous and wind density profiles) even if the bursts in our sample all show a peak in the afterglow light curve (and thus a rising phase).

Note that the same pre–acceleration can occur if the density is homogeneous. In this case, again, we expect the very early afterglow to be less efficient than what predicted without pre–acceleration, leading to a rising phase even harder than t^2.

5 THE SAMPLE

Since we want to study the energetics, luminosities and peak energies of GRBs in the comoving frame, our first requirement is to know the redshift z. Then we also need that the spectral peak energy $E^{\rm obs}_{\rm peak}$ has been determined from the fit of the prompt emission spectrum. Most of these bursts have been localized by the Burst Alert Telescope (BAT; Barthelmy et al. 2005) on board the *Swift* satellite, but only for a few of them BAT could determine $E^{\rm obs}_{\rm peak}$ (due to its limited energy range, 15–150 keV). Most of the $E^{\rm obs}_{\rm peak}$ were determined by the Konus–Wind satellite (Aptekar et al. 1995), or, since mid 2008, by the Gamma Burst Monitor (GBM; Meegan et al. 2009 with energy bandpass 8 keV–35 MeV) on board the *Fermi* satellite. Our sample of GRBs with z and constrained $E^{\rm obs}_{\rm peak}$ (and consequently with computed $E_{\rm iso}$ and $L_{\rm iso}$) is updated up to May

2011. It contains 132 GRBs with z, $E^{\rm obs}_{\rm peak}$ and $E_{\rm iso}$. We have $L_{\rm iso}$ for all but one of these bursts.

Within this sample, we searched the literature for bursts with evidence of the peak of the afterglow or an estimate of the Γ_0 factor:

(i) Liang et al. (2010 – L10 hereafter) measured the peaks in the optical light curves of GRBs and then estimated Γ_0 for the H case. From L10 we collected 9 measurements of $t_{\rm p,z}$. L10 also collected other estimates of $t_{\rm p,z}$ from the literature (their table 6) from which we get other 9 values of this observable. Therefore from L10 we collected 18 estimates of $t_{\rm p,z}$;

(ii) two GRBs, not included in the sample of L10, that show a peak in their optical afterglow light curves are taken from Ghisellini et al. (2009);

(iii) four GRBs, detected by the Large Area Telescope on board *Fermi* at GeV energies, show a peak in their GeV light curves (Ghisellini et al. 2010). Among these there is the short/hard GRB 090510 whose Γ_0 is derived from the modeling of the GeV light curve in Ghirlanda et al. (2010a);

(iv) L10 searched for bursts with evidence of the afterglow peak up to December 2008. Our sample of bursts with redshifts, $E^{\rm obs}_{\rm peak}$ and isotropic energies/luminosities extends to May 2011. We searched in the literature for $t_{\rm p,z}$ of bursts after December 2008 and in 8 cases we could build the light curve with available published data (that will be presented in a forthcoming paper – Melandri et al. 2011).

Our sample is thus composed of 32 GRBs with an estimate of $t_{\rm p,z}$: 31 are long and one is the short GRB 090510 (27 have estimates of $t_{\rm p,z}$ and 5 have upper limits on $t_{\rm p,z}$). The sample is presented in Tab. 1 where we show the relevant properties of these bursts used in the following sections. Col. 1 and 2 show the GRB name and its redshift, Col. 3 the rest frame peak energy $E_{\rm peak}$, and Col. 4 and 5 the isotropic equivalent energy $E_{\rm iso}$ and luminosity $L_{\rm iso}$, respectively. In Col. 6 it is reported the rest frame $t_{\rm p,z}$ from which we compute the Γ_0 factor in the H case (Col. 7) and in the W case (Col. 8) assuming a typical density value $n_0 = 3$ cm^{-3} or $n_0 = 3 \times 10^{35}$cm^{-1} (for the H and W respectively) and a typical radiative efficiency $\eta = 0.2$.

We note from Eq. 15 that the resulting Γ_0 is rather insensitive to the choice of n_0 and η both in the H case [i.e. $\Gamma \propto (n_0\eta)^{-1/8}$] and in the W case [i.e. $\Gamma \propto (n_0\eta)^{-1/4}$].

6 RESULTS

In this section we first show the distributions of the Γ_0 factors computed for the 32 GRBs in the H and W and show the correlation of Γ_0 with the isotropic energy $E_{\rm iso}$ and luminosity $L_{\rm iso}$. Then we show how the distributions of $E_{\rm peak}$, $E_{\rm iso}$ and $L_{\rm iso}$ change when they are corrected for the Γ_0 factor, i.e. how they appear in the comoving frame ($E'_{\rm peak}$, $E'_{\rm iso}$, $L'_{\rm iso}$). In doing this we always consider the two estimates of Γ_0 in the H and W to compare the different distributions of the spectral parameters. Finally, we present the rest frame $E_{\rm peak} - E_{\rm iso}$ and $E_{\rm peak} - L_{\rm iso}$ correlations (updated here with 132 and 131 GRBs up to May 2011) and, for those bursts in our sample with measured Γ_0, we show where they cluster in these planes when the beaming corrections ($E'_{\rm peak} = E_{\rm peak}/(5\Gamma/3)$, $E'_{\rm iso} = E_{\rm iso}/\Gamma$, $L'_{\rm iso} = L_{\rm iso}/(4\Gamma^2/3)$) are applied.

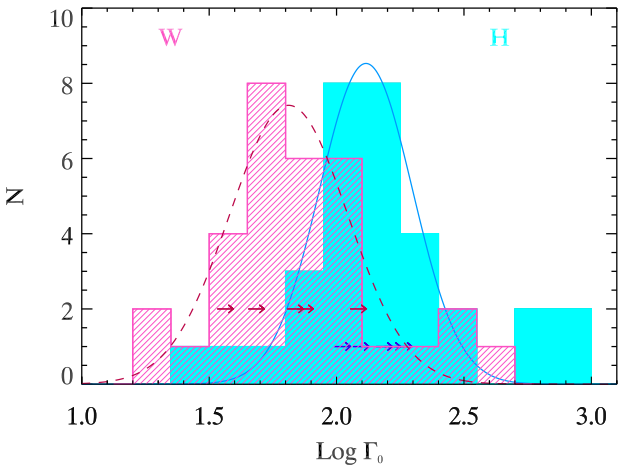

Figure 1. Γ_0 distributions of the 32 GRBs in the case of an homogeneous interstellar medium (H – solid filled blue histogram) and in the case of a wind density profile (W – hatched histogram). The lower limits on Γ_0 (derived from the upper limits on $t_{\rm p,z}$) are shown. The fits with Gaussian functions are also shown with the solid and dashed line for the H and W respectively.

	Parameter	#GRBs	Central value	Dispersion (σ)
	$\log E_{\rm peak}$	132	2.62	0.44
	$\log E_{\rm peak}$	32	2.84	0.48
	$\log E_{\rm iso}$	132	53.05	0.77
	$\log E_{\rm iso}$	32	53.10	0.79
	$\log L_{\rm iso}$	131	52.46	0.73
	$\log L_{\rm iso}$	32	52.53	0.83
Density				
H	$\log \Gamma_0$	32	2.1	0.16
	$\log E'_{\rm peak}$	32	0.42	0.36
	$\log E'_{\rm iso}$	32	51.18	0.71
	$\log L'_{\rm iso}$	32	48.09	0.41
W	$\log \Gamma_0$	32	1.8	0.2
	$\log E'_{\rm peak}$	32	0.71	0.36
	$\log E'_{\rm iso}$	32	51.35	0.49
	$\log L'_{\rm iso}$	32	48.70	0.20

Table 2. Central values and dispersions of the Gaussians fitted to the distributions of Γ_0, $E_{\rm peak}$ and $E'_{\rm peak}$, $E_{\rm iso}$ and $E'_{\rm iso}$, $L_{\rm iso}$ and $L'_{\rm iso}$.

6.1 Γ_0 distributions

Fig. 1 shows the distributions of the Γ_0 factors of the 32 GRBs of our sample (Tab. 1) computed in the H (solid histogram) and W case (hatched histogram), respectively. The two distributions are fitted with Gaussian functions and the central value and dispersion are reported in Tab. 2. The average Γ_0 factor is $\sim$125 in the H case and $\sim$63 in the W case. In both the H and W case the distribution of Γ_0 is broad, spanning more than two decades.

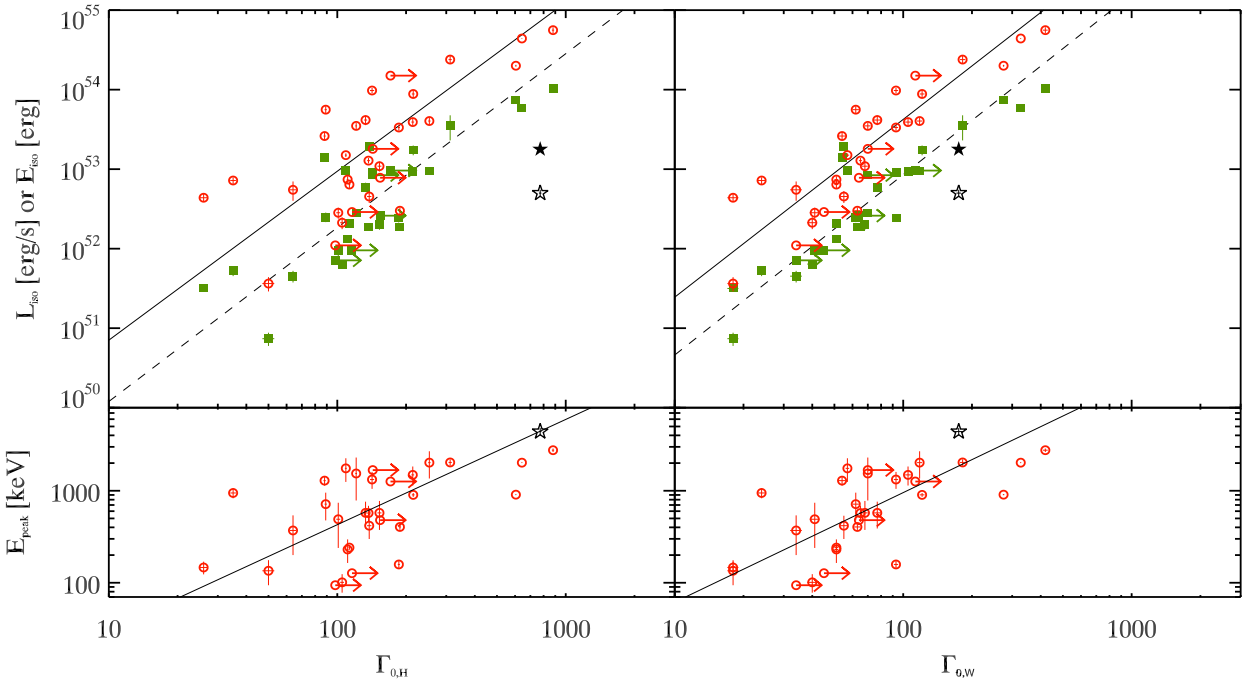

Figure 2. *Top panels:* Isotropic equivalent energy $E_{\rm iso}$ (open red circles) and luminosity $L_{\rm iso}$ (filled green squares) as a function of Γ_0, computed for the 32 GRBs in our sample in the H case (left panel) and W (right panel). The solid (dashed) line in both panels show the least square fit with a power law to the $E_{\rm iso}$–Γ_0 ($L_{\rm iso}$–Γ_0) correlation. *Bottom panels:* Peak energy $E_{\rm peak}$ for the H case (left panel) and W case (right panel) as a function of Γ_0. The solid line is the best fit correlation. The short GRB 090510 is shown separately with the star symbol (filled symbol representing $E_{\rm iso}$ in the top panel and open symbol representing $L_{\rm iso}$ and $E_{\rm peak}$ in the top and bottom panels). The correlation coefficient and the slope and normalization of the best fit correlations are reported in Tab. 3.

6.2 $E_{\rm iso}$–Γ_0, $L_{\rm iso}$–Γ_0, $E_{\rm peak}$–Γ_0 correlations

In this section we explore the presence of correlations between the rest frame GRB properties (i.e. the peak energy $E_{\rm peak}$, the isotropic equivalent energy $E_{\rm iso}$ and luminosity $L_{\rm iso}$) and the Γ_0 factor. A correlation $\Gamma_0 \propto E_{\rm iso}^{0.25}$ was reported by L10 based on their sample of 22 GRBs with estimated Γ_0. Here we show this correlation updated with 32 GRBs and, in addition to this, we present for the first time the correlation of $L_{\rm iso}$ and Γ_0. We also compare these two correlations in the H and W case.

In the upper panels of Fig. 2 we show the isotropic energy $E_{\rm iso}$ and luminosity $L_{\rm iso}$ (open red circles and filled green squares, respectively) as a function of Γ_0 in both the H and W case (left and right panel, respectively). In the bottom panels of Fig. 2 we show the peak energy $E_{\rm peak}$ as a function of Γ_0 in the H (left panel) and W (right panel) case.

The Spearman rank correlation coefficients and associated chance probabilities are reported in Tab. 3. We model the correlations with a power law: $\log Y = m \log \Gamma_0 + q$ (with Y=$E_{\rm iso}$, Y=$L_{\rm iso}$ or Y=$E_{\rm peak}$) and list the best fit parameters in Tab. 3. We fit this model to the data points (shown in Fig. 2) with the bisector method. The choice of this fitting method, instead of the least square Y vs. X method that minimizes the vertical distances of the data from the fitting line, is motivated by the large dispersion of the data and the absence of any physical motivation for assuming that Γ_0 or instead $E_{\rm iso}$, $L_{\rm iso}$ or $E_{\rm peak}$ are the independent variable (Isobe et al. 1990).

We find that there are strong correlations (with significance $> 3\sigma$) between the spectral peak energy and isotropic energy/luminosity with Γ_0. The slopes of these correlations are rather insensitive to the circumburst profile adopted in deriving Γ_0 (H or W) and are similar for $E_{\rm iso}$ and $L_{\rm iso}$ ($E_{\rm iso} \propto {\Gamma_0}^2$ and $L_{\rm iso} \propto {\Gamma_0}^2$). A linear correlation exists between $E_{\rm peak}$ and Γ_0: $E_{\rm peak} \propto \Gamma_0$ (bottom panels in Fig. 2).

Correlation	ρ	$P_{\rm chance}$	m	q	$\sigma_{\rm sc}$
$E_{\rm iso} - \Gamma_0^{\rm H}$	0.7	9×10^{-5}	2.12	48.72	0.24
$L_{\rm iso} - \Gamma_0^{\rm H}$	0.9	2×10^{-9}	2.24	49.15	0.15
$E_{\rm peak} - \Gamma_0^{\rm H}$	0.5	4×10^{-3}	1.14	0.34	0.29
$E_{\rm iso} - \Gamma_0^{\rm W}$	0.8	6×10^{-6}	2.20	47.89	0.20
$L_{\rm iso} - \Gamma_0^{\rm W}$	0.8	10^{-7}	2.26	48.39	0.08
$E_{\rm peak} - \Gamma_0^{\rm W}$	0.7	7×10^{-5}	1.2	0.60	0.26

Table 3. Results of the fit of the Γ_0–$E_{\rm iso}$, Γ_0–$L_{\rm iso}$ and Γ_0–$E_{\rm peak}$ correlations in the two cases of homogeneous insterstellar medium (H) and wind density profile (W). The Spearman correlation coefficient ρ and the chance probability $P_{\rm chance}$ are reported together with the slope m and normalization q of the fit of the data points with a linear model. The fit is done with the bisector method.

The dispersion of the data points around the best fit correlations (shown by the solid and dashed lines in Fig. 2) is modeled with a Gaussian and its $\sigma_{\rm sc}$ is given in Tab. 3. The less dispersed correlation is between the luminosity $L_{\rm iso}$ and Γ_0.

We finally verified that there is no correlation between the GRB duration T_{90} and Γ_0 (chance probability $P = 0.3$ and $P = 0.7$ for the H and W case) and between the redshift z and Γ_0.

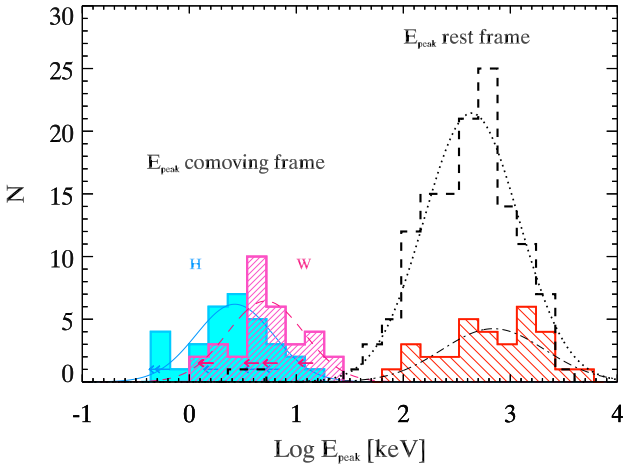

Figure 3. Peak energy distributions in the rest frame $E_{\rm peak}$ (dashed histogram) for the sample of 132 GRBs with known redshift and constrained $E_{\rm peak}$. The hatched histogram shows the 32 GRBs of our sample for which we have an estimate of the peak of the afterglow and hence of Γ_0. The beaming corrected distribution of $E'_{\rm peak}$=$E_{\rm peak}$/(5Γ_0/3) is shown by the solid filled (cyan) histogram in the H case and with the hatched (purple) histogram in the W case. For all the distributions we also show the Gaussian fits whose parameters are reported in Tab. 2 . The 5 upper limits on $E'_{\rm peak}$ (corresponding to lower limits on Γ_0) are also shown with arrows.

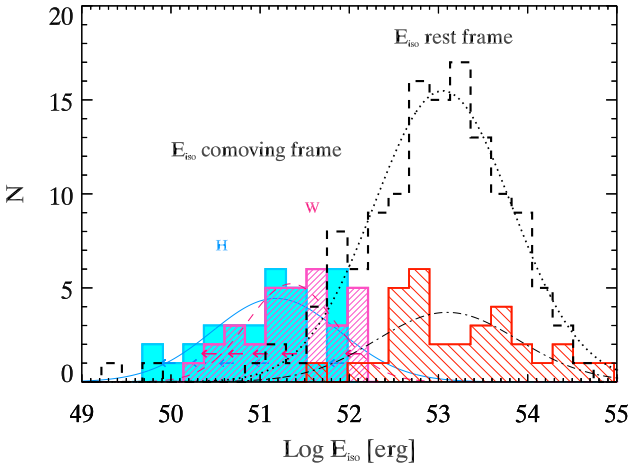

Figure 4. Isotropic energy distributions in the rest frame (dashed histogram) for the sample of 132 GRBs with known redshift and constrained $E^{\rm obs}_{\rm peak}$. The hatched histogram shows the 32 GRBs of our sample for which we have an estimate of the peak of the afterglow. The beaming corrected distribution of $E'_{\rm iso}$=$E_{\rm iso}$/$\Gamma_0$is shown by the solid filled histogram and hatched purple histogram for the H and W case. The 5 upper limits on $E'_{\rm iso}$ (corresponding to lower limits on Γ_0) are also shown with arrows.

6.3 Comoving frame $E'_{\rm peak}$, $E'_{\rm iso}$, $L'_{\rm iso}$ distributions

In Fig. 3, 4 and 5 we show the distributions of the comoving frame peak energy, isotropic equivalent energy and luminosity. In Fig. 3 we show the distributions of the peak energy: the sample of 132 GRBs with measured redshifts and known $E_{\rm peak}$ is shown with the dashed line and the subsample of 32 GRBs of this work for which we could estimate Γ_0 is shown with the red and green hatched histograms. These distributions represent $E_{\rm peak}$, i.e. the peak energy in the rest frame of the sources.

The distributions of the comoving peak energy [derived as $E'_{\rm peak}$=$E_{\rm peak}$/(5Γ_0/3)] are shown by the (cyan) filled and hatched (purple) histograms in Fig. 3 for the H and W case, respectively. Fig. 3 shows also the fits with Gaussian functions: their parameters are reported in Tab. 2.

There is a reduction of the dispersion of the distribution of the peak energy from the rest frame to the comoving one. In the comoving frame $E'_{\rm peak}$ clusters around $\sim$5 keV and $\sim$3 keV in the H and W case, respectively, with dispersions 1.5 decades wide, i.e. narrower than the 2 decades of dispersion of $E_{\rm peak}$.

Fig. 4 shows the distribution of the isotropic energy $E_{\rm iso}$ for all the 132 GRBs with known z and measured $E_{\rm peak}$ (dashed line) and for the 32 GRBs with an estimate of Γ_0 (hatched red histogram). The $E'_{\rm iso}$=$E_{\rm iso}$/Γ_0 distributions are shown with the solid filled (cyan) histogram and the hatched (purple) histogram for the H and W case. The distributions of $E'_{\rm iso}$ are wide and poorly represented by Gaussian functions. On average the comoving frame $E'_{\rm iso}\sim2\times10^{51}$ erg in both the H and W case, but there is a reduction of the dispersion of the distribution of $E_{\rm iso}$ from the rest to the comoving frame values only for the W case (see Tab. 2).

Finally, in Fig. 5 we show the distribution of $L_{\rm iso}$ for the 131 GRBs in the sample (dashed line), the distribution of $L_{\rm iso}$ for the 32 GRBs with estimated Γ_0 (red hatched histogram) and the comoving frame $L'_{\rm iso}$=$L_{\rm iso}$/$(4\Gamma_0^2/3)$ distribution (solid filled and hatched histograms for the H and W case respectively). Interestingly, we find a strong clustering of the comoving frame distribution of $L'_{\rm iso}$. For the H case we find (see Tab. 2 for the values of the Gaussian fits) an average $L'_{\rm iso}\sim 10^{48}$ erg s^{-1} with a small dispersion (0.4 dex), while when using the Γ_0 computed in the wind density profile (W) case we find an almost universal value of $L'_{\rm iso}\sim 5\times10^{48}$ erg s^{-1} with a dispersion of only one order of magnitude around this value (hatched purple histogram and dashed purple line in Fig. 5).

6.4 Comoving frame $E'_{\rm peak}-E'_{\rm iso}$ and $E'_{\rm peak}-L'_{\rm iso}$ correlations

Here we show the effect of correcting the spectral energy correlations $E_{\rm peak}-E_{\rm iso}$ and $E_{\rm peak}-L_{\rm iso}$ for the bulk Lorentz factors Γ_0. These correlations were originally found with a dozen of GRBs (Amati et al. 2002 and Yonetoku et al. 2004 for the $E_{\rm peak}-E_{\rm iso}$ and $E_{\rm peak}-L_{\rm iso}$ correlations respectively) and since then updated with newly discovered GRBs with measured redshifts z and well constrained spectral peak energies $E_{\rm peak}$. In this work we have updated the sample of GRBs with all these observables to May 2011. We have 132 GRBs with measured z and known $E_{\rm peak}$ and $E_{\rm iso}$ and 131 GRBs with measured z and $E_{\rm peak}$ and $L_{\rm iso}$. We show the corresponding $E_{\rm peak}-E_{\rm iso}$ and $E_{\rm peak}-L_{\rm iso}$ correlations in Fig. 6 (left and right panel respectively). The best fit correlation parameters (obtained with the bisector method) are reported in Tab. 4. We find that $E_{\rm peak}\propto E_{\rm iso}^{0.56}$ (dashed line in Fig. 6) with a scatter $\sigma=0.23$ (computed perpendicular to the best fitting line and modeled with a Gaussian function). The other correlation is $E_{\rm peak}\propto L_{\rm iso}^{0.50}$ with a slightly larger scatter $\sigma=0.3$. The 1, 2 and 3σ dispersion of the correlations are shown with the shaded stripes.

Fig. 6 also shows the comoving frame $E'_{\rm peak}$ and $E'_{\rm iso}$ (left panel) and $E'_{\rm peak}$ and $L'_{\rm iso}$ (right panel) for the 32 GRBs of our sample with an estimate of Γ_0 in the H case. Fig. 7 show the same correlations ($E_{\rm peak}-E_{\rm iso}$ and $E_{\rm peak}-L_{\rm iso}$ in the left and right

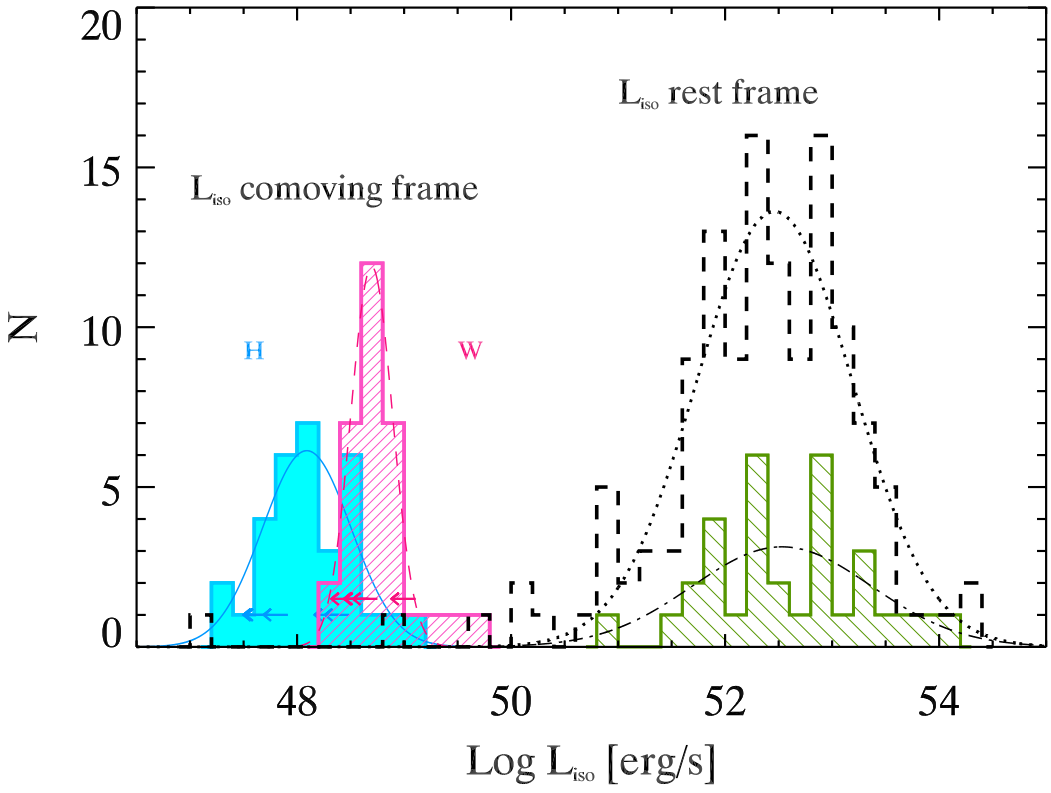

Figure 5. Isotropic luminosity distributions in the rest frame (dashed histogram) for the sample of 131 GRBs with known redshift and constrained $E^{\rm obs}_{\rm peak}$. The hatched histogram shows the 32 GRBs of our sample for which we have an estimate of the peak of the afterglow. The beaming corrected distribution of $L'_{\rm iso}$ is shown by the solid filled histogram and hatched purple histogram for the H and W case. The 5 upper limits on $E'_{\rm iso}$ (corresponding to lower limits on Γ_0) are also shown with arrows.

panels respectively) for the W case. We note that in both the H and W cases there is a clustering of the points around typical values of $E'_{\rm peak}$, $E'_{\rm iso}$ and $L'_{\rm iso}$. Tab. 4 reports the correlation analysis among the comoving frame quantities. We note that in the comoving frame there are no significant residual correlations.

7 DISCUSSION AND CONCLUSIONS

We have considered all bursts with measured $E_{\rm peak}$ and known redshift up to May 2011 (132 GRBs). Among these we have searched in the literature for any indication of the peak of the afterglow light curve $t_{\rm p,z}$ suitable to estimate the initial bulk Lorentz factor Γ_0. Our sample of bursts is composed by 32 GRBs: 27 with a clear evidence of $t_{\rm p,z}$ and 5 upper limits on this observable. We have derived the peak energy $E'_{\rm peak}$, the isotropic energy $E'_{\rm iso}$ and the isotropic peak luminosity $L'_{\rm iso}$ in the comoving frame. To this aim we have derived the general formula for the computation of Γ_0 (§.3) considering two possible scenarios: a uniform interstellar medium density profile (n =const, H) or a wind density profile ($n \propto r^{-2}$, W).

For the wind case the Γ_0-distribution (Fig. 1 and Tab. 2) is shifted at somewhat smaller values ($\langle\Gamma_0\rangle \sim 63$) than the same distribution for the homogeneous density case ($\langle\Gamma_0\rangle \sim 125$). The distribution of $E'_{\rm peak}$ is relatively narrow and centered around $\sim$5 keV (W) or $\sim$ 3 keV for the H case (Fig. 3 and Tab. 2). The distribution of $L'_{\rm iso}$ (Fig. 5) clusters, especially for the wind case, in a very narrow range (less than a decade), around 5×10^{48} erg s^{-1}, while the distribution of $E'_{\rm iso}$ (Fig. 4) is broader ($\sim$2 decades). $E_{\rm iso}$ and $L_{\rm iso}$ correlate with Γ_0, ($\propto {\Gamma_0}^{2.2}$ both for the wind and the homogeneous case) and the correlation is stronger (with a scatter $\sigma = 0.08$) for the wind case. Finally, the duration of the burst, as expected, does not correlate with Γ_0.

These results are schematically summarized in the first column of Tab. 5. The second column of the same table reports some immediate implications of these results. Since $E'_{\rm peak} \propto E_{\rm peak}\Gamma_0$ is contained in a narrow range, all bursts emit their radiation at a characteristic frequency in their comoving frame, irrespective of their bulk Lorentz factor. Furthermore, we can assume that $E_{\rm peak} \propto \Gamma_0$, and this, together with the quadratic dependence on Γ_0 of $E_{\rm iso}$ and $L_{\rm iso}$, yields the "Amati" and the "Yonetoku" relations. *They are the result of a different* Γ_0*–factors.* Indeed, at the extremes of the $E_{\rm peak} - E_{\rm iso}$ and $E_{\rm peak} - L_{\rm iso}$ correlations we find GRB 060218 which has the lowest $\Gamma_0 \sim$ 5 (inferred from its X–ray and optical properties – Ghisellini, Ghirlanda & Tavecchio 2007), while at the upper end (corresponding to the largest peak energies and isotropic energetics and luminosities) there is GRB 080916C which has the largest Γ_0=880.

If all bursts had the same jet opening angle, then $L'_\gamma = \theta_{\rm j}^2 L'_{\rm iso}$, and the (logarithmic) width of the $L'_{\rm iso}$ distribution would be the same of the (more fundamental) L'_γ distribution. On the other hand, we have some hints that very energetic and luminous GRBs tend to have narrower opening angles (e.g. Firmani et al. 2005). It is this property that makes the collimation corrected E_γ and L_γ quantities

	Correlation	# GRBs	ρ	$P_{\rm chance}$	m	q	$\sigma_{\rm sc}$
	$E_{\rm peak}-E_{\rm iso}$	132	0.8	10^{-30}	0.56	-26.94	0.23
	$E_{\rm peak}-E_{\rm iso}$	31	0.8	7×10^{-8}	0.57	-27.78	0.21
	$E_{\rm peak}-L_{\rm iso}$	131	0.8	2×10^{-25}	0.50	-23.05	0.30
	$E_{\rm peak}-L_{\rm iso}$	31	0.8	8^{-7}	0.60	-28.83	0.30
Density	Correlation	# GRBs	ρ	$P_{\rm chance}$	m	q	$\sigma_{\rm sc}$
H	$E'_{\rm peak}$–$E'_{\rm iso}$	31	0.35	7×10^{-2}			
	$E'_{\rm peak}$–$L'_{\rm iso}$	31	0.56	2×10^{-3}			
W	$E'_{\rm peak}$–$E'_{\rm iso}$	31	0.05	8×10^{-1}			
	$E'_{\rm peak}$–$L'_{\rm iso}$	31	0.4	6×10^{-2}			

Table 4. Results of the fit of the $E_{\rm peak}-E_{\rm iso}$ and $E_{\rm peak}-L_{\rm iso}$ correlations updated in this paper to May 2011. We also show the analysis of the possible residual correlation of the $E'_{\rm peak}-E'_{\rm iso}$ and $E'_{\rm peak}-L'_{\rm iso}$ correlations in the H and W case. The Spearman correlation coefficient ρ and the chance probability $P_{\rm chance}$ is given with the slope m and normalization q of the least square fits.

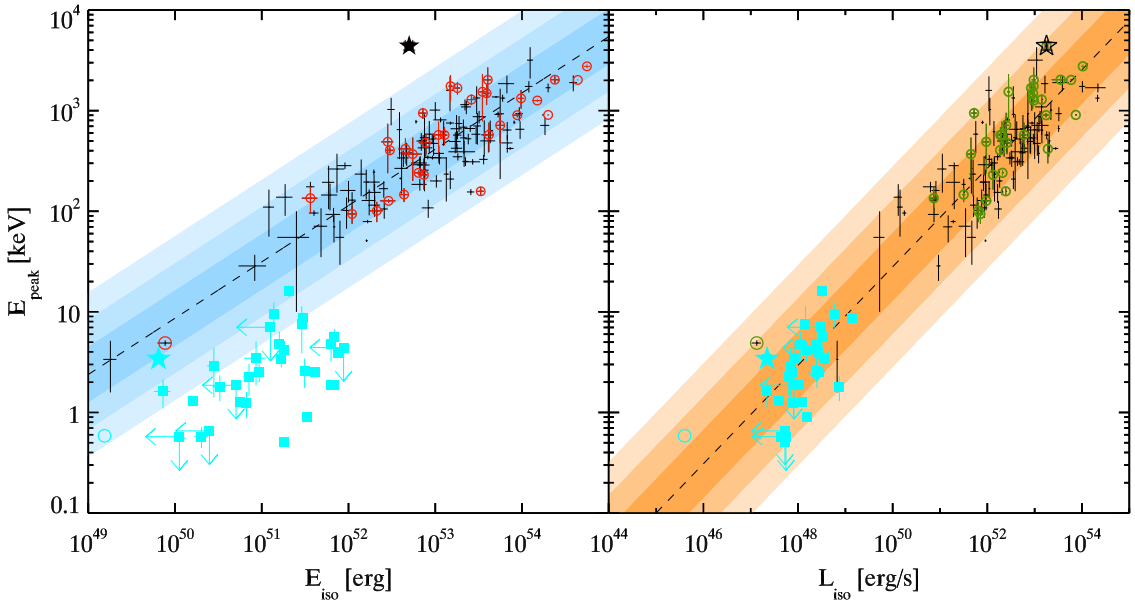

Figure 6. Homogeneous interstellar medium – H. Left: $E_{\rm peak}-E_{\rm iso}$ correlation in the rest frame (crosses and red circles) for 132 GRBs with z and fitted $E_{\rm peak}$ updated to May 2011. Right: $E_{\rm peak}-L_{\rm iso}$ correlation with 131 GRBs. In both panels the best fit correlation is shown by the dashed line and its 1, 2, 3σ scatter is shown by the shaded region. The comoving frame $E'_{\rm peak}$ and $E'_{\rm iso}$ (left) and $E'_{\rm peak}$ and $L'_{\rm iso}$ (right) of 32 GRBs (red open circles [left panel] and green open circles [right panel]) in our sample (Tab. 1) with an estimate of the Γ_0 factor (27 events) or lower limits on Γ_0 (5 events) are shown with the filled cyan square symbols. The short GRB 090510 is also shown with a star symbol and the low luminosity GRB 060218 (with $\Gamma_0\sim5$ [Ghisellini et al. 2006]) is shown with an open circle.

to correlate with $E_{\rm peak}$ in a different way (i.e. different slope) than in the Amati and Yonetoku relation (Ghirlanda et al. 2004; Nava et al. 2006).

We are then led to propose the following ansatz: the opening angle of the jet inversely correlates with the bulk Lorentz factor $\theta_{\rm j}\propto{\Gamma_0}^{-a}$. There are too few GRBs in our sample with measured $\theta_{\rm j}$ to find a reasonable value for the exponent a, but it is nevertheless instructive to explore the case $a=1/2$, leading to $\theta_{\rm j}^2\Gamma_0=$ constant. If we assume this relation we find, for the collimation corrected E_γ:

$$E_\gamma=\theta_{\rm j}^2E_{\rm iso}\propto\Gamma_0\propto E_{\rm peak} \tag{20}$$

This is the "Ghirlanda" relation in the wind case (Nava et al. 2006). Similarly, for the collimation corrected luminosity (Ghirlanda, Ghisellini & Firmani 2006):

$$L_\gamma=\theta_{\rm j}^2L_{\rm iso}\propto\Gamma_0\propto E_{\rm peak} \tag{21}$$

Another important consequence of our ansatz is that, in the comoving frame, the collimation corrected energetic E'_γ becomes constant:

$$E'_\gamma=\theta_{\rm j}^2\frac{E_{\rm iso}}{\Gamma_0}=\ \text{constant} \tag{22}$$

This allows to "re–intepret" the constancy of $L'_{\rm iso}$ as a consequence of the constant E'_γ:

$$L'_{\rm iso}\sim\frac{E'_\gamma}{T'_{90}\theta_{\rm j}^2}=\frac{E'_\gamma}{T_{90}\theta_{\rm j}^2\Gamma_0}=\ \text{constant} \tag{23}$$

In other words, in the comoving frame, the burst emits *the same*

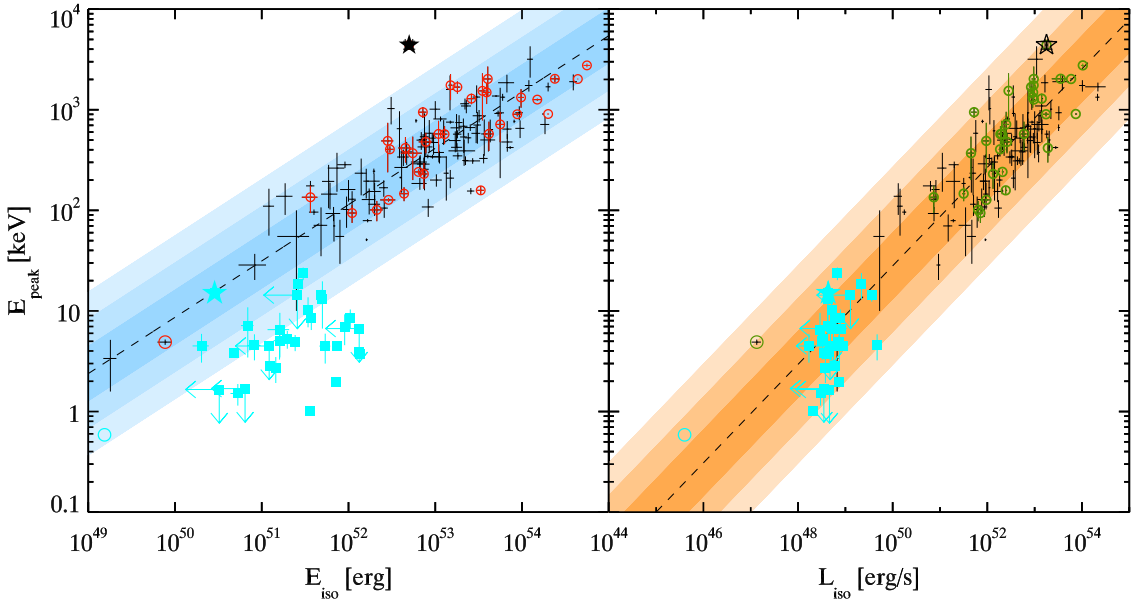

Figure 7. Wind interstellar medium – W. Same as Fig. 6.

amount of energy at the same peak frequency, irrespective of the bulk Lorentz factor. For larger Γ_0 the emitting time in the comoving frame is longer (by a factor Γ_0 if the observed T_{90} is the same), so the comoving luminosity is smaller. But since the jet opening angle is also smaller (for larger Γ_0), the isotropic equivalent luminosity turns out to be the same. These consequences are listed in the third column of Tab. 5.

Interestingly, we note that the general formula for the estimate of the jet opening angle

$$\theta_{\rm j} \propto \left(\frac{t_{\rm j,obs}}{1+z}\right)^{\frac{3-s}{8-2s}} \left(\frac{n_0\eta}{E_{\rm iso}}\right)^{\frac{1}{8-2s}} \qquad (24)$$

with $s = 0$ for the homogeneous case and $s = 2$ for the wind case, can be combined with Eq. 15 to give:

$$\theta_{\rm j}\Gamma_0 \propto \left(\frac{t_{\rm j,obs}}{t_{\rm p,obs}}\right)^{\frac{3-s}{8-2s}} \qquad (25)$$

The product θjΓ_0 then depends only on two observables, i.e. the time of the peak of the afterglow $t_{\rm p,obs}$ and the time of the jet break $t_{\rm j,obs}$, and it is independent from the redshift z and the energetic $E_{\rm iso}$ as well as from the density profile normalization n_0 and radiative efficiency η. If also the product $\theta_{\rm j}^2\Gamma_0$ =const, then we can derive both $\theta_{\rm j} \propto (t_{\rm p,obs}/t_{\rm j,obs})^{\frac{3-s}{8-2s}}$ and $\Gamma_0 \propto (t_{\rm j,obs}/t_{\rm p,obs})^{\frac{3-s}{4-s}}$. If the ansatz $\theta_{\rm j}^2\Gamma_0 = $ const will prove to be true, then by simply measuring the peak time and the jet break time of the afterglow light curve we could estimate both $\theta_{\rm j}$ and Γ_0 for any GRB.

In our sample, only for 4 bursts we can estimate the jet opening angle from the measure of the jet break time of the optical light curve. Their small number does not make possible to directly test the existence of a relation between Γ_0 and $\theta_{\rm j}$. However, an estimate of the jet opening angle can be possible by assuming that all bursts in our sample are consistent with the "Ghirlanda" relation. Fig. 8 shows the estimated $\theta_{\rm j}$ as a function of Γ_0. Stars (squares) refers to angles derived under the assumption of a H (W). To estimate the jet opening angles we considered the most updated "Ghirlanda" correlation, which comprises 29 GRBs with measured jet break time (Ghirlanda et al. 2006). For the homogeneous density profile the relation has the form $\log E_{\rm peak} = -32.81 + 0.70 \log E_\gamma$, while in the case of a W the relation becomes $\log E_{\rm peak} = -50.08 + 1.04 \log E_\gamma$. Given the large scatter of the data points in Fig. 8, we fitted both $\theta_{\rm j}$ versus Γ_0 and Γ_0 versus $\theta_{\rm j}$: we obtain $\theta_{\rm j} \propto \Gamma_0^{-0.37}$ and $\Gamma_0 \propto \theta_{\rm j}^{-1.37}$ for the H case (dashed lines in Fig. 8) and $\theta_{\rm j} \propto \Gamma_0^{-0.63}$ and $\Gamma_0 \propto \theta_{\rm j}^{-1.0}$ for the W case (dot–dashed line in Fig. 8). We conclude that our ansatz $\theta_{\rm j} \propto \Gamma_0^{-1/2}$ is consistent with, but not proven by, this analysis.

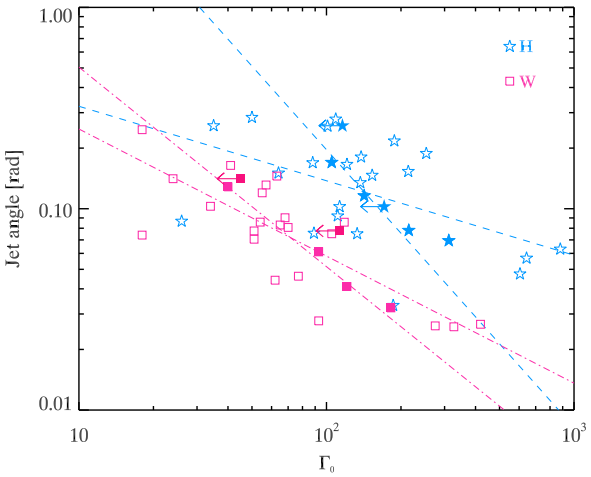

Figure 8. Jet opening angle as a function of Γ_0 for a H (stars) and for a W (squares). Empty symbols show the jet angles estimated by assuming the consistency of our sample with the $E_{\rm peak}$–E_γ relation. Filled symbols refer to the bursts of our sample for which the jet opening angle has been calculated from the measured jet break time of the optical light curves. The two lines (dashed for the H case and dot–dashed for the W case) show the powerlaw fit of the data points considering $\theta_{\rm jet}$ vs Γ_0 and Γ_0 vs $\theta_{\rm jet}$.

An interesting exercise is to estimate the product $\theta_{\rm j}\Gamma_0$. From the observational point of view $\theta_{\rm j}\Gamma \gg 1$ at the end of the prompt

Our results	Implications	If $\theta_{\rm j}^2\Gamma \sim$const
$E'_{\rm peak} \sim$ const	$E_{\rm peak} \propto \Gamma$	
$E_{\rm iso} \propto \Gamma^2$	$E_{\rm iso} \propto E^2_{\rm peak}$	$E_\gamma = \theta_{\rm j}^2 E_{\rm iso} \propto \Gamma \propto E_{\rm peak}$
$L_{\rm iso} \propto \Gamma^2$	$L_{\rm iso} \propto E^2_{\rm peak}$	$L_\gamma = \theta_{\rm j}^2 L_{\rm iso} \propto \Gamma \propto E_{\rm peak}$
T_{90} not $f(\Gamma)$	$T'_{90} \propto \Gamma$	$E'_\gamma \sim$ const
$L'_{\rm iso} \sim$ const	$E'_{\rm iso}/L'_{\rm iso} \propto T'_{90} \propto \Gamma$	$L'_\gamma \sim E'_\gamma/T'_{90} \sim 1/\Gamma$

Table 5. Schematic summary of our results and their implications for the case of a wind density profile. We have assumed that both $E_{\rm iso}$ and $L_{\rm iso}$ scale as Γ^2, instead of $\Gamma^{2.2}$.

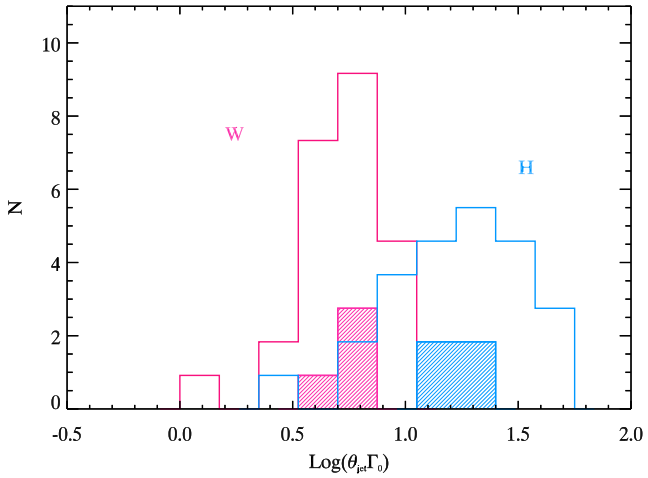

Figure 9. Distribution of $\theta_{\rm j}\Gamma_0$ in the H and W case (blue and purple histograms) estimated by assuming the $E_{\rm peak}$–E_γ relation in the H (Ghirlanda et al. 2004) or W (Nava et al. 2006) case. The hatched histograms show the few GRBs in our samples for which $\theta_{\rm j}$ has been calculated from the measured jet break time in the optical light curve.

phase, so that the decrease of Γ in the afterglow phase, due to the interaction of the GRB fireball with the interstellar medium, gives rise to a jet break when $\theta_{\rm j}\Gamma \sim 1$.

Some numerical simulations (Komissarov et al., 2009) of jet acceleration have shown that a magnetic dominated jet confined by an external medium should have $\theta_{\rm j}\Gamma_0 \leqslant 1$. This value is inconsistent with typical values of $\theta_{\rm j}$ and Γ_0: in the case of an homogeneous wind density profile the typical $\theta_{\rm j} \sim 0.1$ radiants (Ghirlanda et al. 2007) while in the case of a wind density profile $\theta_{\rm j} \sim 0.07$ radiants. Combining these values with the average values of Γ_0 estimated in this paper (Tab. 1) we find $\theta_{\rm j}\Gamma_0 \sim 12$ (5) for the H (W) case.

These are approximate values: the sample of GRBs with measured $\theta_{\rm j}$ (Ghirlanda et al. 2007) contains only 4 bursts of the sample of 32 events of the present paper with estimated Γ_0. However, though somehow speculative, we can derive $\theta_{\rm j}$ for the 32 GRBs of our sample assuming the $E_{\rm peak} - E_\gamma$ correlation in the H case (Ghirlanda et al. 2004) or in the W (Nava et al. 2006). In Fig. 9 we show the distributions of the product $\theta_{\rm j}\Gamma_0$ in the H case (blue histogram) and in the W case (purple histogram). We note that both are centered around typical values of 15 and 5 (for the H and W case, respectively). These values are in good agreement with the results of recent simulations of (i) a magnetized jet confined by the stellar material that freely expands when it breaks out the star (Komissarov, Vlahakis & Koenigl 2010) or (ii) a magnetized unconfined split–monopole jet (Tchekhovskoy, McKinney & Narayan 2009; Tchekhovskoy, Narayan & McKinney 2010). A possible test of these two scenarios could be short GRBs where the absence of the progenitor star would prefer model (ii) for the jet acceleration. In our sample only the short/hard GRB 090510 is present. No jet break was observed for this event and in general we do not yet know if short GRBs follow the same $E_{\rm peak} - E_\gamma$ correlation of long ones.

ACKNOWLEDGMENTS

We acknowledge ASI (I/088/06/0) and a 2010 PRIN–INAF grant for financial support.

REFERENCES

Abdo, A. A., Ackermann, M., Ajello, M., et al., 2009, Nature, 462, 331
Abdo A. A, Ackermann M., Ajello M., et al., 2009a, ApJ, 706, L138
Ackermann M., Asano K., Atwood W.B. et al., 2010, ApJ, 716, 1178
Amati L., Frontera F., Tavani M. et al., 2002, A&A, 390, 81
Amati L., Frontera F. & Guidorzi C., 2009, A&A, 508, 173
Band D.L. & Preece R., 2005, ApJ, 627, 319
Beloborodov A.M., 2002, ApJ, 565, 808
Blandford R.D. & McKee C.F., 1976, Phys. of Fluids, 19, 1130
Bosnjak Z., Celotti A., Longo F. et al., 2008, 384, 599
Butler N.R., Kocevski D., Bloom J.S. & Curtis J.L., 2007, ApJ, 671, 656
Butler N.R., Kocevski D. & Bloom J.S., 2009, ApJ, 694, 76
Chevalier R., Li W., 1999, ApJ, 520, L29
Costa E., Frontera F., Heise J. et al., 1997, Nature, 387, 783
Firmani, C., Ghisellini, G., Ghirlanda, G., et al., 2005, MNRAS, 360, L1
Frail D., Kulkarni S. R.; Nicastro L., et al., 1997, Nature, 389, 261
Ghirlanda G., Ghisellini G., Lazzati D., 2004, ApJ, 616, 331
Ghirlanda G., Ghisellini G., Firmani C., Celotti A. & Bosnjak Z., 2005, MNRAS, 360, 45
Ghirlanda G., Ghisellini G., Firmani C., 2006, NJPh, 8 123
Ghirlanda G., Nava L., Ghisellini G., 2010, A&A, 511, 43
Ghirlanda G., Ghisellini G., Nava L., 2010a, A&A, 510, L7
Ghirlanda G., Ghisellini G., Nava L., Burlon, D., 2011, MNRAS, 401, L47
Ghisellini G., Ghirlanda G., Tavecchio F., 2007, MNRAS, 382, L77
Ghirlanda G., Nava L., Ghisellini G., Firmani C. & Cabrera J.I., 2008, MNRAS, 387, 319
Ghisellini G., Nardini M., Ghirlanda G., Celotti A., 2009, MNRAS, 393, 253
Ghisellini G., Ghirlanda G., Nava L., Celotti A., 2010, MNRAS, 403, 926
Gruber, D., Kruehler, T., Foley, S., et al., 2011, A&A, 528, 15
Hascot R., Vennin V., Daigne F., Mochkovitch R., 2011, arXiv1101.3889
Isobe T., Feigelson E. D., Akritas M. G., Babu G. J., 1990, ApJ, 364, 104
Komissarov S. S., Vlahakis N., Koenigl A., Barkov, Maxim V., 2009, MNRAS, 394, 1182
Komissarov S. S., Vlahakis N., Koenigl A., 2010, MNRAS, 407, 17
Krimm H.A., Yamaoka K., Sugita S. et al., 2009, ApJ, 704, 1405
Liang E.-W.; Yi S.-X.; Zhang, J., 2010, ApJ, 725, 2209
Lithwick Y.; Sari R., 2001, ApJ, 555, 540

Molinari E., Vergani, S. D., Malesani, D., et al., 2007, A&A, 469, L13
Nakar, E. & Piran, T., 2005, MNRAS, 360, L73
Nava L., Ghisellini G., Ghirlanda G., et al., 2006, 450, 471
Nava L., Ghirlanda G., Ghisellini G. & Firmani C., 2008, MNRAS, 391, 639
Panaitescu A., Kumar P., 2000, ApJ, 543, 66
Sari R., 1997, ApJ, 489, L37
Sari R., Piran T., 1999, ApJ, 520, L17
Shahmoradi, A. & Nemiroff, R. J., 2011, MNRAS, 411, 1843
Tchekhovskoy A., McKinney J. C., Narayan R., 2009, ApJ, 699, 1789
Tchekhovskoy A., Narayan R., McKinney J. C., NewA, 2010, 15, 749
Yonetoku, D., Murakami, T., Nakamura, T. et al. 2004, ApJ, 609, 935
Wijers R. A. M. J. & Galama T. J., 1999, ApJ, 523, 177
Zhao X.-H., Li Z., Bai J.-M., 2011, ApJ, 726, 89
Zou Y.-C., Piran T., et al., 2010, MNRAS, 402, 1854
Zou, Y.-C., Fan, Y.-Z., Piran T., 2011, ApJ, 726, L2